Petroleum Science 23 (2026) 7416–7428

Contents lists available at ScienceDirect

Petroleum Science

journal homepage: www.keaipublishing.com/en/journals/petroleum-science

Original Paper

Rheological behavior and disulfide bond-mediated self-degradation of dual-network hydrophobically associated polyacrylamide fracturing fluid

Xin Wen [a,*], Gui-Qiang Fei [a], Hua-Qiang Shi [b], Yi-Jie Jiang [b], Guang-Liang Jia [c,d], Jiao-Jiao Zhu [e], Qian-Qian Liu [a], Cheng Wang [f], Xiao-Juan Lai [a], Lei Wang [a]

[a] Key Laboratory of Auxiliary Chemistry and Technology for Chemical Industry, Ministry of Education, Shaanxi University of Science & Technology, Xi'an, 710021, Shaanxi, China
[b] National Engineering Laboratory for Exploration and Development of Low-Permeability Oil & Gas Fields, Oil & Gas Technology Research Institute Changqing Oilfield Company, Xi'an, 710021, Shaanxi, China
[c] China University of Geosciences, Wuhan, 430074, Hubei, China
[d] Sinopec North China Petroleum Engineering Co., Ltd., Zhengzhou, 450000, Henan, China
[e] SNF Well (Xi'an) Technology Co., Ltd., Xi'an, 710021, Shaanxi, China
[f] SNF (China) Flocculant Co., Ltd., Taixing, 225400, Jiangsu, China

ARTICLE INFO

Article history:
Received 10 February 2026
Received in revised form
13 August 2026
Accepted 14 August 2026
Available online 19 August 2026

Edited by Yan-Hua Sun

Keywords:
Self-degradation
Dual-network
Hydrophobically associated polyacrylamide
Degradation kinetics
Fracturing fluid

ABSTRACT

To improve the rheological properties of polyacrylamide-based fracturing fluids, a common approach is to increase the amount of copolymer; however, this inevitably leads to greater damage to reservoirs. In this study, a self-degradable polyacrylamide (DS-PAM) with high rheological performance was synthesized, featuring disulfide bonds and a dual-network structure (physicochemical structure). The as-prepared fracturing fluid had excellent temperature-shear resistance (>50 mPa·s) and viscoelasticity ($G' > G''$) at 100 °C and 40,000 mg/L salinity. More importantly, kerosene facilitates the "competitive capture" of hydrophobic groups, causing dissociation of the hydrophobic associative network. Concurrently, hydrolysis of disulfide bonds triggers cleavage of the covalent network, while high temperature provides sufficient activation energy for the degradation reaction, accelerating the scission of molecular chains. The degradation process follows the pseudo-first-order kinetic model. Under the synergic effects of physical network dissociation and chemical network cleavage, degradation products with molecular weight less than 200,000 are achieved within 48 h. The scaling rate (<0.5%) and core damage (19.8%) of the degradable fluid are substantially reduced, which is highly significant for reservoir protection.
© 2026 The Authors. Publishing services by Elsevier B.V. on behalf of KeAi Communications Co. Ltd. This is an open access article under the CC BY-NC-ND license (http://creativecommons.org/licenses/by-nc-nd/4.0/).

1. Introduction

Fracturing fluid is hailed as the "blood" of hydraulic fracturing, and its rheological properties directly determine the conductivity of artificial fractures as well as oil and gas production (Huang et al., 2020; Ismail and Azadbakht, 2024). Increasing copolymer dosage is a common strategy for improving the rheological properties of polyacrylamide-based fracturing fluids (Gupta et al., 2003). However, copolymer degradation requires additional gel breakers (APS, V_c) (Ghosh et al., 2021), the resulting anions, SO_4^{2-} and CO_3^{2-}, react with divalent cations such as Ca^{2+}, Mg^{2+}, Ba^{2+}, and Sr^{2+} in formation water to form sparingly or slightly soluble scale deposits, which plug formation pores (Telin et al., 2023). Moreover, conventional polyacrylamide fracturing fluid systems generate substantial amounts of flocculent residues, which readily cause flocculation, leading to pore structure damage, reduced fracture conductivity, and severe secondary reservoir damage (Gao et al., 2023; Yang et al., 2023).

To address the problem of aggravated reservoir damage caused by increased polymer dosage, numerous studies have been conducted. Among the available solutions, polymer modification is the most effective strategy, and existing research mainly focuses on the following two aspects.

* Corresponding author.
E-mail address: 5252@sust.edu.cn (X. Wen).
Peer review under the responsibility of China University of Petroleum (Beijing).

https://doi.org/10.1016/j.petsci.2026.08.017
1995-8226/© 2026 The Authors. Publishing services by Elsevier B.V. on behalf of KeAi Communications Co. Ltd. This is an open access article under the CC BY-NC-ND license (http://creativecommons.org/licenses/by-nc-nd/4.0/).

(1) Construction of a crosslinked dual-network structure. Almubarak et al. (2019) developed a dual-network polymer fracturing fluid composed of guar gum derivatives and polyacrylamide for high temperature reservoirs, which significantly mitigated formation damage. He et al. (2024) synthesized a polyacrylic acid-polyacrylamide (PAA/PAM) dual-network hydrogel, which exhibited excellent strength, water absorption capacity, and swelling ratio, demonstrating great application potential in profile control, water shutoff, and flooding operations.
(2) Grafting of functional monomers. Liu et al. (2024) prepared hydrophobically modified polyacrylamide (HPAAB) by introducing the hydrophobic monomer behenyl alcohol polyoxyethylene ether methacrylate into PAM, which exhibited excellent performance under various pH, temperature and shear rate conditions. Narimani et al. (2022) prepared a crosslinked hydrogel of AM-co-AMPS/GO via graft copolymerization of AM and AMPS onto hydroxypropyl guar gum (HPG), followed by reinforcement with graphene oxide (GO). This hydrogel exhibited significantly enhanced salt tolerance, shear resistance, and thermal stability.

However, these modification strategies enable polymers to maintain favorable rheological properties even at low dosages and make the polymer structure more stable and less susceptible to degradation, thus failing to resolve the contradiction between performance enhancement and reservoir damage reduction.

Dynamic covalent bonds (imine bonds and disulfide bonds) enable the rearrangement of polymer networks under specific conditions, endowing the polymers with self-degradability (Campos et al., 2025; Maruya et al., 2020). Zhang et al. (2024a) prepared a bio-based material (PGCS-100) via the grafting reaction between 4-formylbenzoic acid and peach gum polysaccharide with –CHO groups in its side chains (PGP-CHO). PGCS-100 contains dynamic imine bonds, which can be completely degraded under acidic conditions (Zhang et al., 2024b). Wang et al. (2022) designed a double-crosslinked PAM based on dynamic covalent Schiff base bonds, which enabled crosslinking point cleavage in acidic reservoir environments (pH < 4), with a 40% higher degradation rate than conventional systems. Takahashi et al. (2016) synthesized bis(4-glycidyloxyphenyl) disulfide (BGPDS) using bis(4-hydroxyphenyl) disulfide and epichlorohydrin, yielding a diepoxy group containing disulfide bonds. External stimuli (light or temperature) induce the formation of free radicals, which cleave the disulfide bonds and enable the polymer to degrade into smaller fragments. Moreover, to uniformly distribute dynamic covalent bonds along the molecular chains, reversible addition-fragmentation chain transfer (RAFT) polymerization was used to synthesize the target polymer (Hess et al., 2020). This polymerization method enables efficient regulation of the polymer's molecular weight, molecular weight distribution, and structural characteristics (Rosenbloom et al., 2021; Shao et al., 2020; Wang et al., 2023). It also endows the polymer with high chain-end fidelity, and further achieves self-degradability (Moad et al., 2005).

Herein, a self-degradable dual-network hydrophobically associated polyacrylamide (DS-PAM) was synthesized via RAFT polymerization. The first network, formed by physical associations between hydrophobic groups, endows the polymer with excellent rheological properties (Ye et al., 2020), while the second network, constructed via dynamic covalent crosslinking, enables its self-degradability (Jing et al., 2019). Furthermore, the effect of monomer concentration on DS-PAM performance was comprehensively analyzed, and reservoir damage evaluation was conducted on the degradation solution. The as-prepared fracturing fluid exhibits both excellent rheological properties (η > 50 mPa·s) and self-degradation within 48 h without the addition of a breaker (degradation products with molecular weight less than 200,000), providing a theoretical basis and technical reference for the green development of oil and gas fields in unconventional reservoirs.

2. Experimental section

2.1. Materials

N,*N*′-Bis(acryloyl)cystamine (BAC, AR), acrylamide (AM, AR), acrylic acid (AA, AR), and sodium hydroxide (NaOH, AR) were purchased from Shanghai Macklin Biochemical Technology Co., Ltd. Diallyl dimethyl ammonium chloride (CK-3, AR) was sourced from Shanghai Yuanye Biotechnology Co., Ltd. Dithiocarbamate (DTC, AR), sodium hypophosphite (HYPO, AR), tert-butyl hydroperoxide (TBHP, AR), ascorbic acid (V_c, AR), 2,2′-azobis(2-methylpropionamidine) dihydrochloride (V50, AR), sodium chloride (NaCl, AR), potassium chloride (KCl, AR), calcium chloride ($CaCl_2$, AR), magnesium chloride ($MgCl_2$, AR), ammonium persulfate (APS, AR), and ethylenediaminetetraacetic acid disodium salt (EDTA-2Na, AR) were purchased from Sinopharm Chemical Reagent Co., Ltd. Hydrolyzed polyacrylamide (HPAM, T.P.) was sourced from Shaanxi Runtai Chemical Industry Co., Ltd. Acetone (C_3H_6O, AR) and anhydrous ethanol (C_2H_6O, AR) were purchased from Tianjin Hongyan Chemical Reagent Factory. Brine, composed of 2.0% KCl, 5.5% NaCl, 0.45% $MgCl_2$, and 0.55% $CaCl_2$, was prepared for evaluating the properties of water-based DS-PAM. Unless otherwise stated, all aqueous solutions used throughout the experiments were prepared with deionized water.

2.2. Design of self-degradable polyacrylamide

To enhance the performance of polyacrylamide (PAM) as a fracturing fluid in complex environments and to impart self-degradability, the following strategy was adopted: (1) Acrylamide (AM) was used as the molecular backbone, and the hydrophobic monomer diallyl dimethyl ammonium chloride (CK-3) was grafted onto it to form a physically associated network, thus imparting hydrophobic association properties to the polymer. (2) *N*,*N*′-Bis(acryloyl)cystamine (BAC) was incorporated into the polymer to form a chemically crosslinked network, enhancing the temperature resistance, salt resistance, and shear resistance of the polymer and reducing formation damage. This is mainly attributed to the strong hydrophobicity of the long-chain alkyl groups ($–C_{17}H_{33}$) at the terminals of CK-3, these hydrophobic groups tend to aggregate spontaneously, forming hydrophobic association microdomains, namely physically crosslinked networks. Meanwhile, the acryloyl groups (–CO–CH=CH_2) at both ends of BAC molecules can be grafted onto the molecular backbones via covalent bonds during the polymerization process, forming chemically crosslinked networks between molecular chains and enabling the construction of a dual-network (Fig. 1). In addition, disulfide bonds (S–S) contained in BAC can be cleaved under specific conditions, thereby endowing PAM with self-degradability and achieving the goal of reducing formation damage.

2.3. Characterization

The chemical structure of the samples was characterized using a VECTOR-22 Fourier transform infrared (FT-IR) spectrometer (Bruker Corporation, Germany) with a wavenumber range of 4000–500 cm^{-1}. The analyte was dissolved in deuterium oxide (D_2O), and the dissolved sample was transferred to a specialized nuclear magnetic resonance (NMR) tube. The proton NMR spectrum was determined using a nuclear magnetic resonance

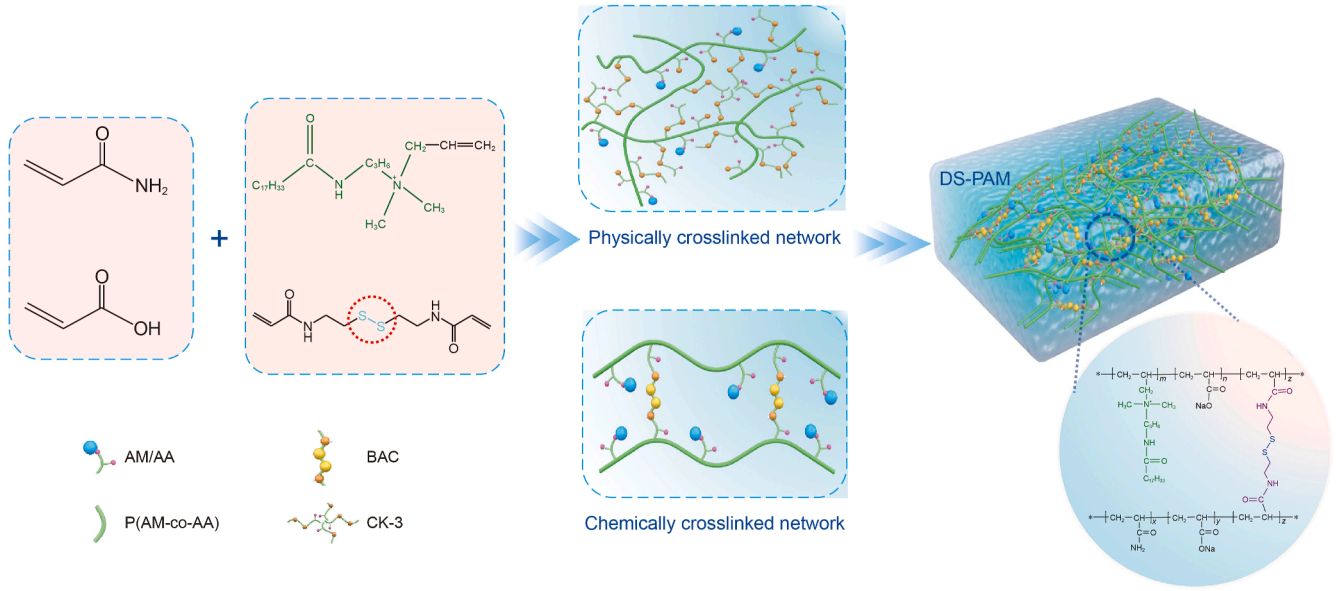


Fig. 1. Design concept of self-degradable polyacrylamide (DS-PAM).

spectrometer (AVANCE III, Bruker Corporation, Germany). The morphological properties of the samples were characterized using a field-emission scanning electron microscope (FEI Verios 460, FEI Company, USA) operated at 15 kV. Thermogravimetric analysis (TGA) was performed using a Discovery TGA thermogravimetric analyzer (TA Instruments). The particle size distribution of DS-PAM fluids at different concentrations was determined by dynamic light scattering (DLS) with a wide-angle laser light scatterometer (Brookhaven, BI200SM, Suffolk, NY, USA).

2.4. Rheological properties

The shear stability of the DS-PAM fluids at elevated temperatures was measured on a HAAKE MARS rheometer with a cylinder at 170 s^{-1} and different temperatures of 90, 100, and 120 °C. The angular frequency sweep (0.1–10 Hz) and the creep behavior of DS-PAM fluids with different salinities were conducted on an Anton Paar MCR 302 rheometer equipped with CP50-1-SN 30644 plate fixture, having a diameter of 0.099 mm, at room temperature (26 °C). Notably, the salinity in this work only originates from the cations (Na^+, K^+, Ca^{2+}, Mg^{2+}) in the brine, which consists of 2.0% KCl, 5.5% NaCl, 0.45% $MgCl_2$, and 0.55% $CaCl_2$.

2.5. Degradation behavior and kinetic models

The number-average molecular weight (M_n) and weight-average molecular weight (M_w) of both the pristine and degraded samples were determined using gel permeation chromatography (GPC) (Pitt and Gu, 1987; Zhao et al., 2022). The measurements were performed on a Polymer Laboratory PL-GPC 50 chromatograph equipped with a refractive index detector, column oven, and auto-sampler. An Aquagel-OH 60 column was used at 30 °C, with 0.1 mol/L $NaNO_3$ as the mobile phase at a flow rate of 0.5 mL/min. Calibration was carried out using polyethylene glycol (PEG) standards ($k = 12.5 \times 10^{-3}$ mL/g, $\alpha = 0.78$). Additionally, the micromorphology of the degraded materials was observed using scanning electron microscopy (SEM).

Molecular weight distribution index (PDI) can be calculated as follows:

$$\mathrm{PDI} = \frac{M_w}{M_n} \tag{1}$$

where M_w is the weight-average molecular weight; M_n is the number-average molecular weight.

Degradation kinetic models were employed to investigate the degradation mechanism of DS-PAM, and the corresponding formula is as follows:

Pseudo-first-order kinetic model (Pitt et al., 1981):

$$\ln M_{n_t} = \ln M_{n_0} - K_1 t \tag{2}$$

Pseudo-second-order kinetic model (Li et al., 2025a):

$$\frac{1}{M_{n_t}} - \frac{1}{M_{n_0}} = K_2 t \tag{3}$$

where M_{n_t} is the number-average molecular weight at time t; M_{n_0} is the initial molecular weight ($t = 0$); t is the degradation time, h; K_1 and K_2 are apparent rate constants.

3. Results and discussion

3.1. Characterization and molecular weight analysis

The viscosity of DS-PAM increases continuously with increasing BAC concentration (Fig. S3). When the BAC concentration exceeds 0.3 mol/L, the structural crosslinking density of DS-PAM exceeds 97% and the viscosity rises above 160 mPa·s, leading to poor solution solubility (Fig. S3(a)). Viscosity profiles for CK-3 concentration of 0.2, 0.4, and 0.6 mol/L, all exhibit abrupt transitions, with critical association concentrations (C^*) of 0.26%, 0.20%, and 0.12%, respectively (Fig. S3(b)). Below C^*, intramolecular association predominates, and polymer chains remain coiled; above C^*, the effective concentration of hydrophobic monomers increases, promoting intermolecular association and network formation, which causes a sharp increase in solution viscosity (Grassl et al., 2001). Therefore, 0.3 mol/L of BAC and 0.4 mol/L of CK-3 were selected as the optimal formulation parameters (Fig. S3(c) and (d)).

The CK-3 and DS-PAM were characterized using infrared spectroscopy (Fig. 2(a)). For DS-PAM, the characteristic absorption peaks at 3200–3500 cm^{-1} correspond to the N–H stretching vibrations of the amide group (–NH_2) in acrylamide and the O–H stretching vibrations of the carboxyl group (–COOH) in acrylic acid. This confirms that the monomers, acrylamide and acrylic acid, were successfully polymerized into DS-PAM. The absorption band observed at approximately 3080 cm^{-1} in the CK-3 spectrum, attributed to the C–H stretching vibration of the allyl group (=C–H), disappears in DS-PAM, indicating that the CK-3 monomer was almost completely consumed in the polymerization reaction. The band at 1720–1700 cm^{-1} in the DS-PAM spectrum corresponds to the C=O stretching vibration of the carboxyl group (–COOH) in acrylic acid, verifying the incorporation of the acrylic acid monomer into DS-PAM. Most notably, a new characteristic absorption peak appears in the DS-PAM spectrum within the 500–600 cm^{-1} range. This peak is assigned to the stretching vibration of the disulfide bond (S–S) in BAC, providing definitive evidence that BAC was successfully grafted into the DS-PAM structure. In summary, the infrared spectra verify that the molecular structure of the synthesized polymer matches the designed structure.

The CK-3 and DS-PAM were characterized using ^1H NMR (Fig. 2(b)). The newly emerged characteristic signals in the DS-PAM spectrum at approximately 3.00 ppm and 8.05–8.10 ppm are attributed to the protons of methylene groups linked by disulfide bonds (–CH_2–S–S–CH_2–) and the amide group (–$CONH_2$), respectively. This provides conclusive evidence that BAC has been successfully grafted onto the DS-PAM backbone. The resonance signals observed in the range of 1.00–1.30 ppm correspond to the protons of methylene (–CH_2–) and methine (–CH–) groups, confirming the successful incorporation of acrylamide and acrylic acid into the DS-PAM structure. The characteristic peak at approximately 1.80 ppm in the CK-3 spectrum, which is assigned to the protons on the unreacted olefinic double bond (–CH_2–C=C–CH_2–), vanishes in the DS-PAM spectrum. This demonstrates that the CK-3 monomer has been successfully polymerized into DS-PAM. In summary, these observations confirm that BAC and CK-3 have been successfully incorporated into the polymer.

Thermogravimetric analysis (TGA) results of DS-PAM and HPAM are presented in Fig. 2(c). The TG curves show that both polymers exhibit a gradual decrease in residual mass as the temperature increases, stabilizing above 480 °C. DS-PAM has a lower final residual mass than HPAM, indicating its inferior thermal stability. To endow DS-PAM with self-degradation performance, dynamic covalent bonds (S–S) were introduced into its molecular structure. These bonds are prone to breaking at high temperatures,

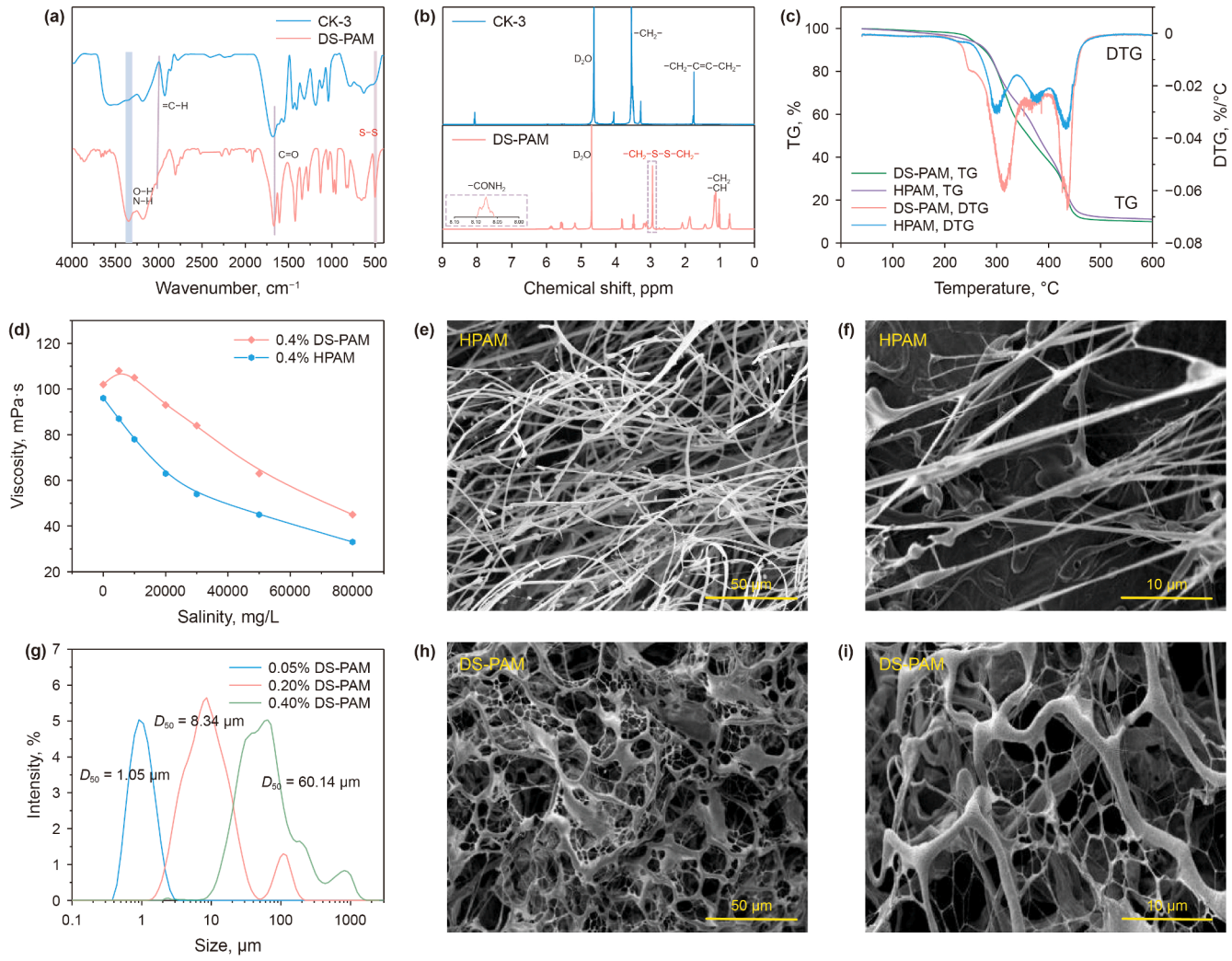


Fig. 2. (**a**) FT-IR spectra of CK-3 and DS-PAM; (**b**) ^1H NMR spectra of CK-3 and DS-PAM; (**c**) TG and DTG curves of DS-PAM; (**d**) effect of salinity on viscosity of DS-PAM and HPAM; (**e**, **f**) SEM images of HPAM; (**g**) DLS size distribution of DS-PAM at 0.05%, 0.20% and 0.40%; (**h, i**) SEM images of DS-PAM.

thereby reducing the thermal stability of DS-PAM. In the DTG curves, HPAM displays two distinct negative peaks at 300 and 420 °C, signifying high thermal stability since decomposition occurs only at elevated temperatures. The relatively small peak intensities indicate a mild thermal degradation process. In contrast, DS-PAM shows sharper negative peaks with greater intensities at the same temperatures, demonstrating more vigorous decomposition and a stronger thermal degradation potential.

As salinity increases, the viscosity of HPAM decreases monotonically from 96 to 33 mPa·s. In contrast, the viscosity of DS-PAM first rises slightly from 102 to 108 mPa·s and then declines to 45 mPa·s (Fig. 2(d)). This difference arises from their distinct molecular structures. HPAM chains are rich in hydrophilic carboxyl groups (–COOH). Added salt ions screen the electrostatic repulsion between charged chains, reducing the hydrodynamic volume and thus lowering viscosity. DS-PAM contains hydrophobic groups that form micelle-like associative domains. At moderate salinity, charge screening promotes intermolecular hydrophobic association, creating reversible physical crosslinks that increase viscosity (Zhong et al., 2007; Zhou et al., 2010). However, further increases in salt concentration disrupt these hydrophobic domains, tighten chain coiling, and partially dissociate the physical network, leading to the eventual viscosity drop (Zhang and Li, 2022). In addition, DS-PAM exhibits a critical salt concentration. At low salinity, salt ions enhance hydrophobic association, resulting in an increase in viscosity. After exceeding the critical point, the electrostatic shielding effect of ions causes the molecular network to coil, thereby reducing the viscosity.

Dynamic light scattering (DLS) measurements of DS-PAM at different concentrations are presented in Fig. 2(g). The particle size increases with polymer concentration. At a concentration of 0.05%, a small, unimodal distribution is observed (D_{50} = 1.05 μm), indicating that intramolecular association dominates in this dilute regime. At a concentration of 0.2%, the size increases (D_{50} = 8.34 μm) and the distribution broadens as more chains form larger aggregates. At a concentration of 0.4%, above the critical association concentration, intermolecular association becomes dominant, leading to large supramolecular aggregates (D_{50} = 60.14 μm), a broadened profile and secondary peaks, consistent with the formation of a polydisperse entangled network.

HPAM exhibits a relatively smooth, slender fibrous morphology, with its chain segments maintaining an essentially linear distribution (Fig. 2(e) and (f)). The surface lacks obvious pores, indicating the absence of strong physical crosslinking between the molecular chains of HPAM; its structure is maintained only by electrostatic repulsion or a small amount of chemical crosslinking. DS-PAM forms physical crosslinking points through intermolecular or intramolecular associations of the introduced CK-3 hydrophobic monomers in the aqueous phase (Fig. 2(h) and (i)), thereby constructing a primary network. Simultaneously, a secondary network is established via covalent crosslinking between molecular chains through the introduced BAC monomers. This “physical-chemical” double crosslinking mechanism induces significant microphase separation and a three-dimensional network, endowing DS-PAM with a hierarchical structure characterized by abundant pores, distinct skeletons, and remarkable structural heterogeneity.

To evaluate the difference in molecular weight between HPAM and DS-PAM, the intrinsic viscosity method was employed to calculate the molecular weights of the polymers, with the specific results presented in Table S1. The molecular weight of HPAM is markedly higher than that of DS-PAM. HPAM can reach the tens of millions range, owing to the small size of acrylamide and its linear polymerization pattern, facilitated by optimized process conditions that minimize steric hindrance and allow unobstructed chain growth. In contrast, during DS-PAM polymerization, the long alkyl chains of the hydrophobic monomer CK-3 introduce significant steric hindrance at the growing chain end, shielding the active radical center and slowing propagation. Furthermore, the chemical crosslinker BAC alters chain growth from linear to branched, forming a three-dimensional network. This topological constraint further restricts chain extension (Zhang et al., 2025), resulting in a lower molecular weight of DS-PAM. Thus, the molecular weight of DS-PAM is lower than that of HPAM.

3.2. Rheological property analysis

To evaluate the viscosity–temperature behavior of the 0.4% DS-PAM solution (Fig. 3(a)), the temperature was increased from 30 to 90 °C, then to 100 and 120 °C. The apparent viscosity of the DS-PAM solution decreased with rising temperature. At maximum temperatures of 90, 100, and 120 °C, the apparent viscosities were 64, 55, and 41 mPa·s, respectively. This is because the elevated temperature intensified molecular thermal motion, which disrupted intermolecular entanglements and broke hydrogen bonds, driving the molecular chains into a state of “free slippage” (Bai et al., 2022), resulting in a rapid viscosity decline.

A comparative assessment of temperature and shear resistance of HPAM and DS-PAM was conducted (Fig. S4). A 0.4% DS-PAM solution maintained viscosities of 56, 52, and 26 mPa·s at 90, 100, and 120 °C after 60 min of shearing at 170 s^{-1}, indicating favorable shear stability of the polymer. At constant temperature and shear rate, chain orientation reached saturation; further orientation had minimal influence on viscosity, and the system entered a state of “shear-orientation equilibrium” with stable viscosity. When the temperature rose to 120 °C, the disulfide bonds in the BAC covalent crosslinks cleaved upon heating, leading to the disintegration of the covalent crosslinking network. This caused a significant loss of the polymer's functionality as a thickener or structural material. Such damage was irreversible, resulting in permanent reduction of molecular weight and loss of performance. Therefore, DS-PAM had a temperature threshold for shear stability, beyond which degradation occurred. In contrast, the HPAM system maintained high viscosity even under continuous shearing at 120 °C and 170 s^{-1} (Fig. S4(c)), demonstrating the favorable high-temperature degradability of DS-PAM.

To evaluate the salt resistance of DS-PAM, the viscosity was measured at different salinities (10,000, 40,000, and 80,000 mg/L) (Fig. 3(b)), yielding final viscosities of 65, 20, and 11 mPa·s, respectively. Under low-salinity conditions, charge screening reduces the electrostatic repulsion between polymer segments, facilitating closer proximity of hydrophobic groups, thereby further strengthening the associative network and increasing viscosity. Under high-salinity conditions, metal ions disrupt the electric double layer structure induced by hydrogen bonding between polymer molecules and water molecules, reducing intermolecular attraction and consequently weakening the network structure of the solution.

To evaluate the viscosity recoverability of DS-PAM after high-shear treatment, the recovery performance of the solution was measured at 90 °C under shear rates of 170, 300, 500, and 1000 s^{-1} (Fig. 3(c)). DS-PAM achieved a viscosity recovery rate of 98.4%, compared with 86.2% for HPAM. Unlike HPAM, whose viscosity loss results from irreversible chain disentanglement and scission under high shear, DS-PAM dissipates shear energy via the dynamic breakage and recombination of hydrophobic association sites, preserving its covalent crosslinked framework and backbone integrity to exhibit superior shear resistance (Jiao et al., 2023; Liu et al., 2021).

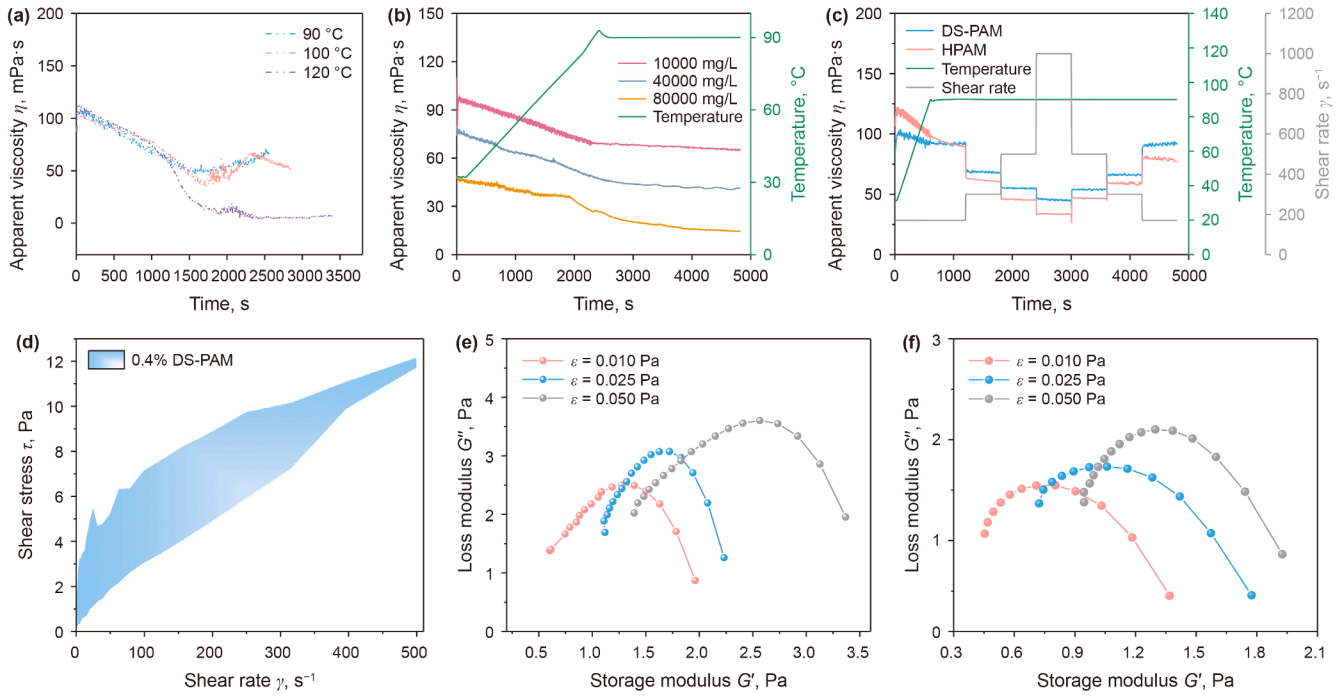


Fig. 3. Rheological stability of DS-PAM: (**a**) effect of temperature on the viscosity of DS-PAM (at a shear rate of 170 s^{-1}); (**b**) effect of salinity on the viscosity of DS-PAM (at a shear rate of 170 s^{-1}); (**c**) effect of shear intensity on the viscosity of DS-PAM and HPAM; (**d**) thixotropy of DS-PAM; (**e**) Cole-Cole plot (freshwater); (**f**) Cole-Cole plot (saline solution). ε is the strain.

The thixotropic curves of DS-PAM are presented in Fig. 3(d). With increasing DS-PAM concentration, the shear stress increases significantly, and the curve shape transitions from approximately linear to nonlinear, indicating that DS-PAM exhibits shear-thickening behavior and effectively maintains viscoelasticity under high shear conditions. At a DS-PAM concentration of 0.4%, the shear stress rises sharply (>12 Pa), and the rheological curve displays nonlinear characteristics with a distinct yield stress plateau in the low-shear-rate region, demonstrating high rigidity that requires critical stress to disrupt the static structure. Shear forces "disengage" hydrophobic microdomains, causing polymer chains to orient and disentangle along the flow direction, which results in a significant reduction in flow resistance and a sharp drop in viscosity (Li et al., 2022). At high shear rates, the physically associated network is completely disrupted, and the viscosity is dominated by contributions from the solvent, polymer concentration (Li et al., 2025b), and friction between stretched polymer chains, reaching a lower plateau. When the shear rate decreases, hydrophobic groups reaggregate (Kaewsaiha et al., 2005), the network structure self-heals, and viscosity recovery exhibits a lag, forming a thixotropic loop. The thixotropic area expands with increasing DS-PAM concentration, as confirmed by the results for 0.05% and 0.20% DS-PAM (Fig. S5(a) and (b)). Thus, DS-PAM possesses excellent shear resistance and recovery capability.

To evaluate the viscoelasticity of DS-PAM under different environmental conditions, the linear viscoelastic region (LVR) was first determined through stress sweep measurements. Both in freshwater and saline solution, DS-PAM exhibited predominantly elastic behavior when the storage modulus (G') was larger than the loss modulus (G''), with G' and G'' remaining nearly parallel within a specific stress range that corresponds to LVR of DS-PAM (Fig. S5(c)). Based on this, frequency sweep tests were subsequently performed in both freshwater and saline solution to measure the variations of G' and G'' with frequency, and Cole-Cole plots were constructed accordingly (Fig. 3(e) and (f)). Within the tested frequency range, both the G' and G'' increased with rising frequency. This phenomenon mainly arises because at low frequencies, the network structure deforms slowly and the molecular chains have sufficient relaxation time, remaining in a low-energy state. Most energy is dissipated through viscous flow, resulting in a low storage modulus G'. As the frequency increases, the network structure deforms rapidly, leaving insufficient time for molecular chain slippage. The network's capacity for energy storage is thus continuously enhanced, leading to a gradual increase in G'. In saline environments, ions are dispersed among molecules, enhancing solution polarity and further strengthening hydrophobic associations between chains (Liu et al., 2025), which reinforces the solution network structure and endows DS-PAM with excellent viscoelasticity. However, excessively high frequencies eventually overcome the constraints of hydrophobic associations, causing the dissociation of hydrophobic microdomains and the rapid collapse of the physically crosslinked network, which results in a sharp decline in both G' and G''.

3.3. Self-degradability of DS-PAM

This study analyzed the influence of varying kerosene concentrations on the viscosities of DS-PAM solutions (Fig. 4(a)). As the kerosene concentration increases, the viscosities of DS-PAM solutions with different concentrations continuously decrease, indicating that the addition of kerosene can induce the degradation of DS-PAM. In contrast, HPAM only undergoes physical phase separation without degradation in the presence of kerosene. This difference arises because, when oil droplets are dispersed in the DS-PAM solution, oil molecules act as a "preferred solvent" for hydrophobic groups (Duncke et al., 2026). Kerosene dissolves the hydrophobic groups on the DS-PAM molecular chains, resulting in the "competitive capture" of these hydrophobic groups by the oil phase and leading to the dissociation of the hydrophobic association network of DS-PAM.

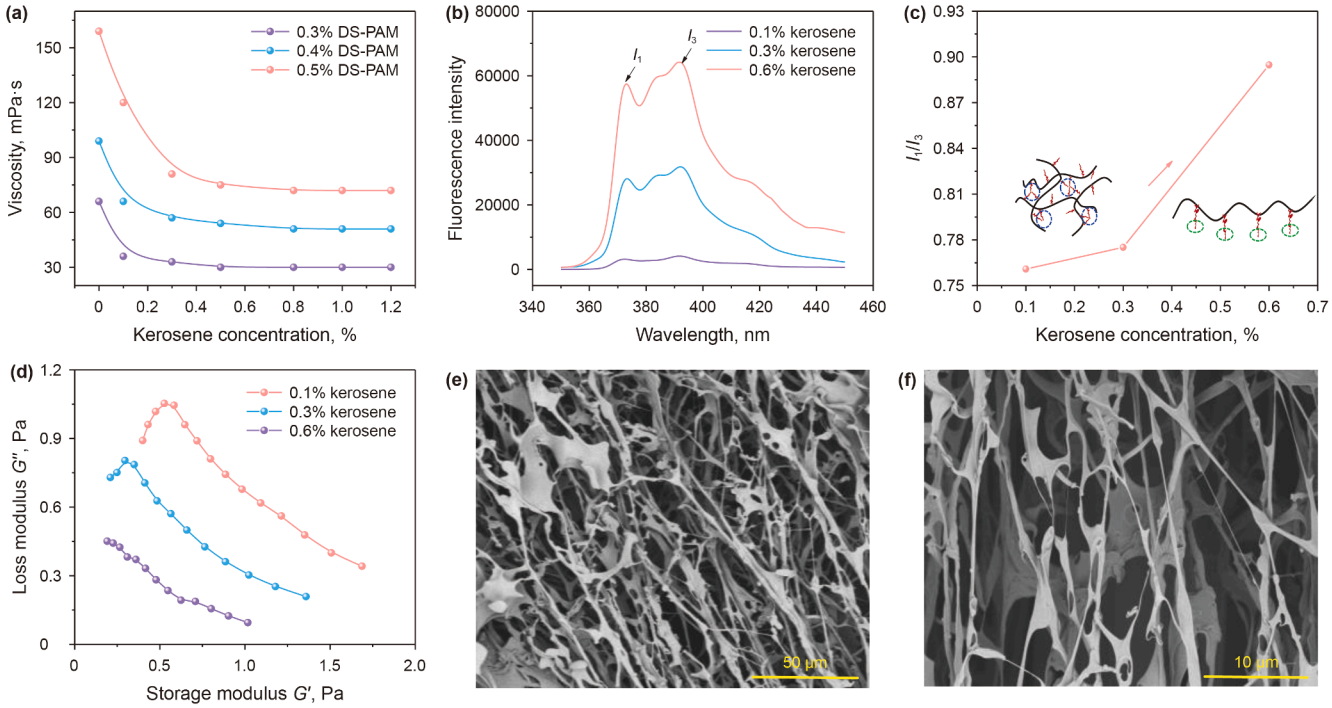


Fig. 4. (**a**) Effect of kerosene concentrations on the viscosity of DS-PAM; (**b**) fluorescence spectra of DS-PAM at different kerosene concentrations; (**c**) effect of kerosene concentrations on I_1/I_3 value of DS-PAM; (**d**) Cole-Cole plot of DS-PAM at different kerosene concentrations; (**e**, **f**) SEM images of DS-PAM after the addition of kerosene.

I_1/I_3 refers to the fluorescence intensity ratio between the first and third vibrational peaks of the pyrene monomer in fluorescence spectra, which reflects the hydrophobicity of the microenvironment in the solution. A lower I_1/I_3 value indicates stronger hydrophobicity of the microenvironment (Fischer et al., 1998). As the kerosene concentration increases, the I_1/I_3 ratio continuously rises, indicating that the polarity of the microenvironment decreases significantly and the hydrophobicity continues to enhance (Fig. 4(b)). There exists a "critical oil concentration" (C_0) for the degradation of DS-PAM (Fig. 4(c)). When the oil phase concentration is lower than C_0, the increase in the I_1/I_3 ratio is gradual, and the destructive effect of oil droplets on the crosslinked network of DS-PAM is limited, which is insufficient to disrupt the entire network. However, when the oil phase concentration exceeds C_0, the destructive effect of oil droplets is significantly enhanced, leading to the gradual dissociation of the three-dimensional network of DS-PAM (Fig. 4(e) and (f)) and triggering a sharp decrease in solution viscosity (Zhang et al., 2024b). The nonpolar molecules in the oil phase possess a stronger affinity for the hydrophobic groups of DS-PAM, which disrupts the physically crosslinked network and induces the collapse of the dual-network structure, manifesting macroscopically as a substantial reduction in the viscosity and viscoelasticity of the solution.

The Cole-Cole plot of DS-PAM at different kerosene concentrations is shown in Fig. 4(d). As the kerosene concentration increased from 0.1% to 0.6%, both G' and G'' of the system gradually decreased, indicating that the addition of kerosene weakened hydrophobic associations of DS-PAM, resulting in the dissociation of the physically crosslinked network between polymer chains. This may be attributed to the strong hydrophobicity of kerosene, which disrupts the topological structure of the hydrophobic associative network through competitive adsorption and swelling effects (Sun et al., 2023). The higher the kerosene concentration, the deeper the degree of network dissociation, ultimately leading to the transition of the system from a gel state to a dilute solution.

At all tested temperatures, the viscosity of DS-PAM decreased with increasing degradation time (Fig. 5(a)). This indicates that scission of the molecular chains of DS-PAM occurs, leading to a reduction in molecular weight and consequently a decrease in viscosity. At 30 °C, the viscosity of DS-PAM decreases from 102 to 79 mPa·s within 240 h, indicating that the viscosity of DS-PAM decreases slowly under ambient temperature. At 120 °C, the viscosity drops from an initial value of 102 to 9 mPa·s within 48 h, and after 120 h, it decreases to below 5 mPa·s. It is evident that within the same degradation time, the higher the temperature, the greater the viscosity reduction amplitude of DS-PAM, the faster the degradation rate. This is because high temperature provides sufficient activation energy for the degradation reaction, accelerating the scission of the molecular chains of DS-PAM (Santos et al., 2024).

Under different pH values, the viscosity of DS-PAM decreases with the extension of degradation time, indicating that the degradation of DS-PAM is affected by pH (Fig. 5(b)). At pH 7, the viscosity of DS-PAM decreases from 102 mPa·s to approximately 10 mPa·s within 144 h, indicating that the viscosity of DS-PAM decreases relatively slowly under neutral conditions. At pH 6, the viscosity drops from 102 mPa·s to about 10 mPa·s in 120 h, demonstrating that the viscosity reduction of DS-PAM under acidic conditions is faster than that under neutral conditions. At pH 8, the viscosity decreases from 102 mPa·s to roughly 10 mPa·s within 72 h, indicating that the viscosity of DS-PAM decreases the fastest under alkaline conditions. It can be seen that acidic or alkaline environments can accelerate the degradation of DS-PAM (Fig. S6(a)–(c)). This is because the neutral system lacks sufficient H^+ or OH^- ions to participate in the reaction, leading to the inhibition of disulfide bond hydrolysis. In contrast, in the alkaline

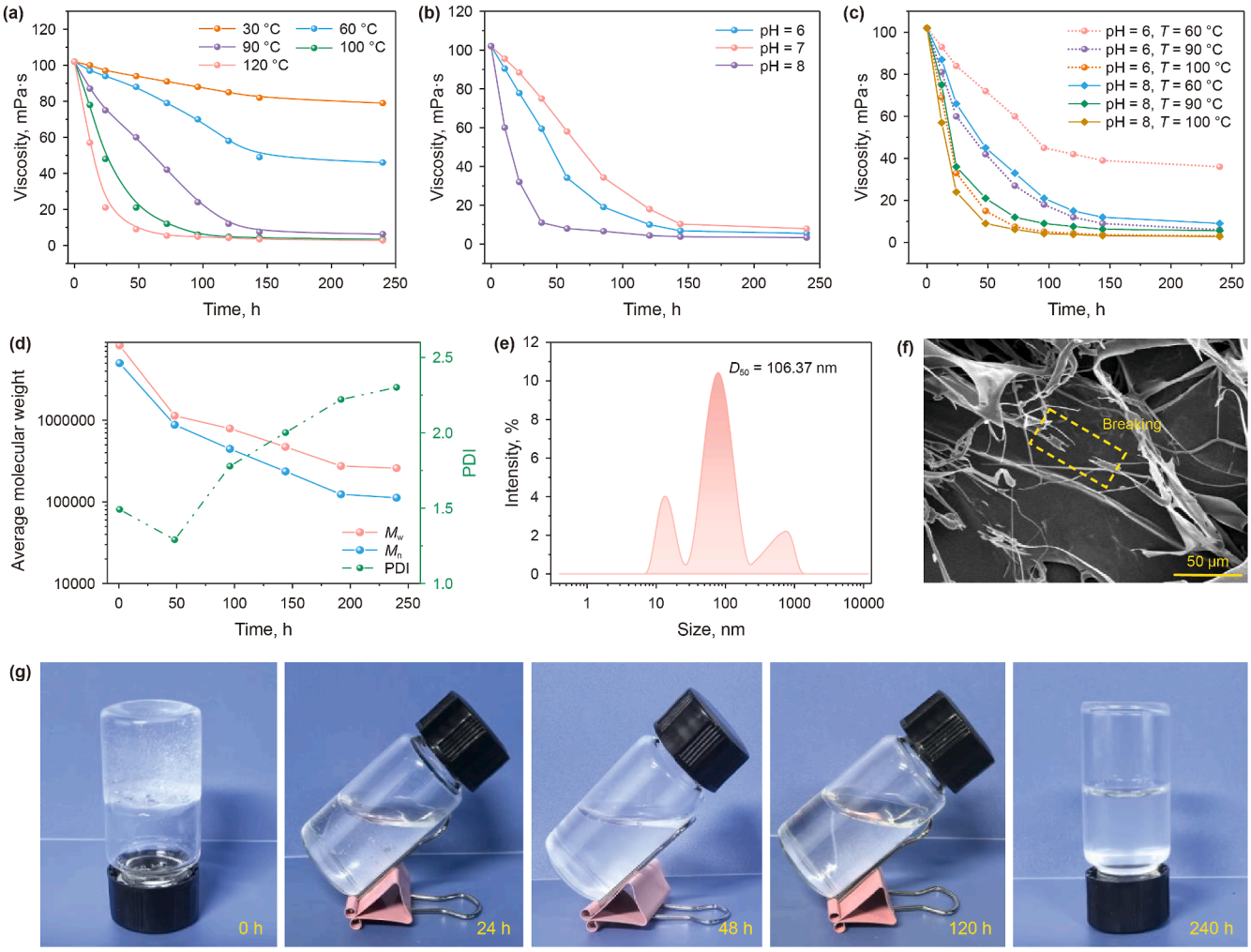


Fig. 5. Effects of temperature (**a**), pH (**b**), and pH–temperature synergy (**c**) on viscosity of DS-PAM; (**d**) changes in the number-average molecular weight (M_n), weight-average molecular weight (M_w), and polydispersity index (PDI, PDI = M_w/M_n) of DS-PAM during degradation; (**e**) particle size of DS-PAM during 240 h of degradation; (**f**) SEM images of DS-PAM under the synergistic effect of pH and temperature; (**g**) photographs of DS-PAM recorded at 0, 24, 48, 120, and 240 h of degradation.

environment (Fig. 5(f)), OH^- ions can accelerate the scission of disulfide bonds, triggering the depolymerization of the polymer molecular chains, thereby disrupting the integrity of the three-dimensional network and promoting the degradation of DS-PAM.

pH and temperature can synergistically affect the degradation of DS-PAM (Fig. 5(c)). In terms of the amplitude and rate of viscosity change, under the conditions of pH 8 and 100 °C, the viscosity decreases from 102 mPa·s to approximately 10 mPa·s within 48 h, indicating that the viscosity decreases most rapidly under these conditions. Furthermore, at the same temperature, the decrease rate of viscosity at pH 8 is consistently higher than that at pH 6. At the same pH, the higher the temperature, the faster the decrease rate, which is consistent with the previous analysis results. Interestingly, at pH 8, it takes 72 h for the viscosity to decrease to 10 mPa·s; at 100 °C, it also takes 72 h for the viscosity to drop to 10 mPa·s. However, under the combined conditions of pH 8 and 100 °C, only 48 h are required for the viscosity to decrease to 10 mPa·s, and the viscosity reduction is further accelerated (Fig. 5(g)). This is because the polymer molecular chains of DS-PAM simultaneously undergo the dual effects of structural weakening caused by pH-induced dissociation and reaction acceleration driven by high temperature, which renders the three-dimensional network more susceptible to disruption and thus accelerates the degradation of DS-PAM.

With increasing time, both the number-average molecular weight (M_n) and weight-average molecular weight (M_w) continue to decrease (Fig. 5(d)). Before degradation, both the M_n and M_w of DS-PAM are over one million, attributed to the long molecular chains of DS-PAM. However, as the degradation time increases, both M_n and M_w decrease to below 200,000, which is due to the scission of the molecular chains of DS-PAM with the extension of degradation time. Furthermore, it can be observed that the molecular weights decrease rapidly within the first 48 h and then gradually slow down. This indicates that a large number of molecular chains undergo scission in the early stage of degradation, leading to a rapid reduction in molecular weights. After 48 h, the difficulty of scission for the remaining molecular chains increases, resulting in a slower rate of molecular weight decrease. More importantly, throughout the entire degradation process, the M_w of DS-PAM is consistently greater than the M_n, indicating that the degradation of DS-PAM is disordered. Furthermore, the polydispersity index (PDI, PDI = M_w/M_n) first decreases and then gradually increases during the degradation of DS-PAM. This indicates that in the early stage of degradation (within 48 h), the

disulfide bonds on the BAC monomers introduced via RAFT polymerization are preferentially degraded, leading to chain shortening. However, as the degradation time extends (after 48 h), the disulfide bonds are exhausted, and the degradation shifts to random scission, thereby generating a large number of oligomers and short-chain fragments.

The average particle size of DS-PAM before degradation is 106.37 nm (Fig. 5(e)), while after degradation, it decreases to 58.37 nm, which is only one-thousandth of that before degradation. Furthermore, the particle size distribution curve of the degraded product exhibits only one peak, indicating that the degraded product exhibits a concentrated particle size distribution range with no large particle residues. It can also be observed from the cumulative distribution curve that all particle sizes of the degraded product have decreased to the nanoscale. Thus, the degraded product can migrate through the pores of reservoir rocks, achieving the goal of reducing reservoir damage.

3.4. Degradation kinetics analysis of DS-PAM

To investigate the degradation mechanism of DS-PAM, the M_n of the polymer under different pH values and temperatures over the entire degradation period were analyzed.

The pseudo-first-order degradation kinetic equations of DS-PAM at different temperatures are shown in Fig. 6(a). The goodness of fit (R^2) values for the pseudo-first-order kinetic model fitting of DS-PAM are all greater than 0.9 at 30 60, 90, 100, and 120 °C. This indicates a strong linear relationship between $\ln(M_{n_0}/M_{n_t})$ and time, confirming that the degradation of DS-PAM follows the pseudo-first-order kinetic model. Meanwhile, as the temperature increases, the slope of the fitting line gradually increases, indicating that higher temperature accelerates the degradation of DS-PAM. Among these temperatures, the pseudo-first-order kinetic equation exhibits the highest R^2 value (0.969) at 100 °C, demonstrating the best correlation for the degradation kinetics under this condition. Although the slope is the largest at 120 °C, the corresponding R^2 value (0.943) is lower than that at 100 °C (0.969). This may be attributed to 120 °C exceeding the optimal temperature for the temperature and shear resistance of DS-PAM, resulting in performance variations that interfere with the degradation reaction and reduce the goodness of fit of the model.

The pseudo-first-order degradation kinetic equations of DS-PAM at different pH values are shown in Fig. 6(b). The R^2 values for the pseudo-first-order kinetic model fitting of the three data sets corresponding to pH values of 6, 7, and 8 are all greater than 0.9. This indicates a strong linear relationship between $\ln(M_{n_0}/M_{n_t})$ and time. The slope of the fitting equation for the pseudo-first-order kinetic model is 0.018 at pH 6, 0.015 at pH 7, and 0.024 at pH 8. This indicates that the degradation rate of DS-PAM is the fastest at pH 8 and the slowest at pH 7. This

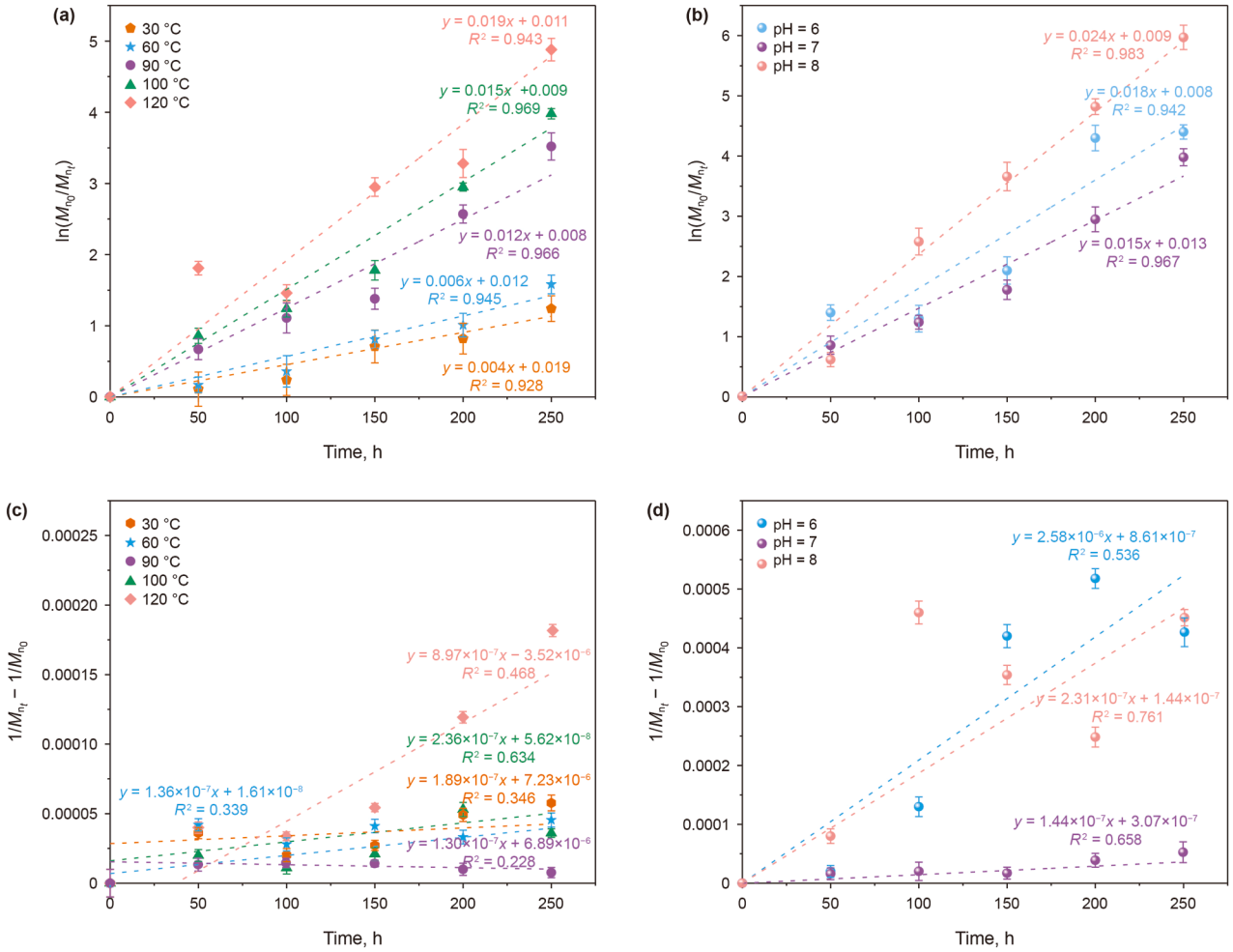


Fig. 6. Pseudo-first-order and pseudo-second-order kinetic fitting of DS-PAM degradation under varying conditions: (**a**) pseudo-first-order fitting at different temperatures; (**b**) pseudo-first-order fitting at different pH values; (**c**) pseudo-second-order fitting at different temperatures; (**d**) pseudo-second-order fitting at different pH values.

difference is primarily due to the effect of pH on the generation of free radicals involved in the degradation process of DS-PAM. The system at pH 8 is more conducive to the formation of highly reactive free radicals, which can continuously and effectively attack the polymer molecular chains of DS-PAM, thereby accelerating its degradation.

The pseudo-second-order degradation kinetic equations of DS-PAM at different temperatures and pH values, respectively, are shown in Fig. 6(c) and (d). The R^2 values for the pseudo-second-order kinetic model fitting of DS-PAM are all less than 0.9 at varying temperatures and pH values. This indicates that the degradation of DS-PAM does not conform to the pseudo-second-order kinetic model, further demonstrating that the degradation process is not dominated by a simple bimolecular reaction mechanism. Instead, it is dominated by the intramolecular attack of certain components (H^+/OH^-) in the medium on the chemical bonds (disulfide bonds) within DS-PAM, which is an unimolecular process. The degradation rate depends only on the concentration of the DS-PAM polymer chains themselves.

3.5. Self-degradation mechanism of DS-PAM

The degradation of DS-PAM essentially stems from its unique dual-network structure. This process occurs through the synergistic effects of environmental factors such as oil phase, pH, and temperature, which induce the dissociation of the physically associated network and the scission of the chemically crosslinked network. Ultimately, this process leads to self-degradation (Fig. 7). More importantly, these two processes occur synchronously, with the cleavage of the chemical network contributing more significantly than the dissociation of the physical network. This is attributed to the fact that the covalent network resides within the polymer main chains; its rupture severs the polymer into fragments, resulting in a substantial viscosity reduction (Fig. 5(c)). In contrast, the dissociation of the hydrophobic association network leaves the backbone intact, leading to a relatively minor change in viscosity (Fig. 4(a)).

Before degradation, DS-PAM was composed of a chemically crosslinked network and a physically associated network (Fig. 7(a)). In the presence of kerosene, oil molecules competitively bound to the hydrophobic groups ($-C_{17}H_{33}$), leading to the dissociation of intermolecular hydrophobic microdomains and the collapse of the physically crosslinked network (Fig. 7(b)). More importantly, the dissociation of the physical network opened channels for the subsequent degradation of the covalent network, fully exposing the chemical crosslinking points (S–S bonds) inside the DS-PAM network (Fig. 7(e)). This significantly reduced the steric hindrance of the chemical reaction and created conditions for the complete degradation of the chemical network.

The S 2*p* spectrum shows a prominent S^{6+} characteristic doublet at 168–170 eV after degradation (Fig. 8(b)), indicating that high temperature and pH cleaved the disulfide bonds (S–S), with the degradation product being sulfonate groups (SO_3^{2-}), which further confirms the degradation of the chemically crosslinked network. The scission of disulfide bonds (S–S) is an intramolecular or intrachain unimolecular process that does not require collisions with other molecules. Its rate depends only on the concentration of disulfide bonds within the DS-PAM polymer chains themselves (the degradation of DS-PAM conforms to the pseudo-first-order kinetic model). Meanwhile, the intensities of the O–C=O and C–O peaks in the C 1*s* spectrum increased significantly (Fig. 8(c) and (e)), and the C–N and C–NH_2 peaks in the N 1*s* spectrum rose in intensity and shifted (Fig. 8(d)), demonstrating that the cleavage of the DS-PAM main chain –CH_2–CH($CONH_2$) generated abundant oxygen-containing carbon groups (–COOH, –OH) and amino groups (–NH_2). In addition, the degradation of the chemically crosslinked network caused the remaining physical association sites to lose all support completely (Fig. 8(f)). The two effects occurred synchronously, mutually reinforcing each other and collectively driving the self-degradation of DS-PAM.

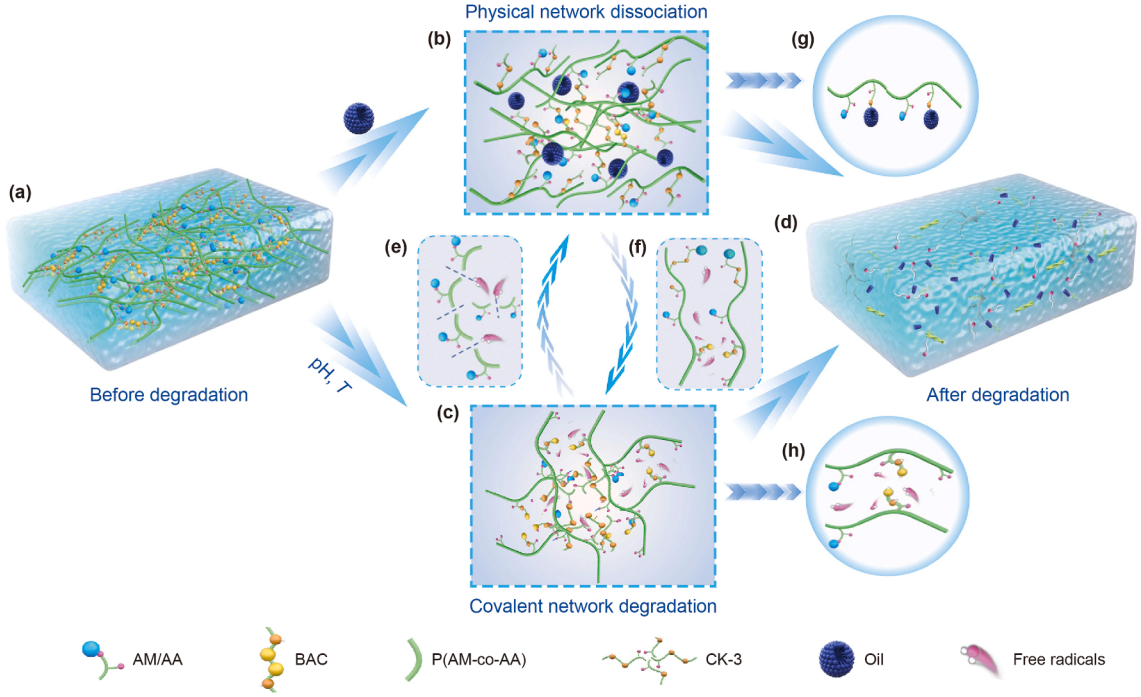


Fig. 7. (**a**) DS-PAM before degradation; (**b**) physical network dissociation; (**c**) covalent network degradation; (**d**) DS-PAM after degradation; (**e**) covalent network degradation promotes physical network dissociation and induces molecular chain scission; (**f**) physical network dissociation accelerates covalent network cleavage; (**g**) magnified view of physical network dissociation; (**h**) magnified view of covalent network degradation.

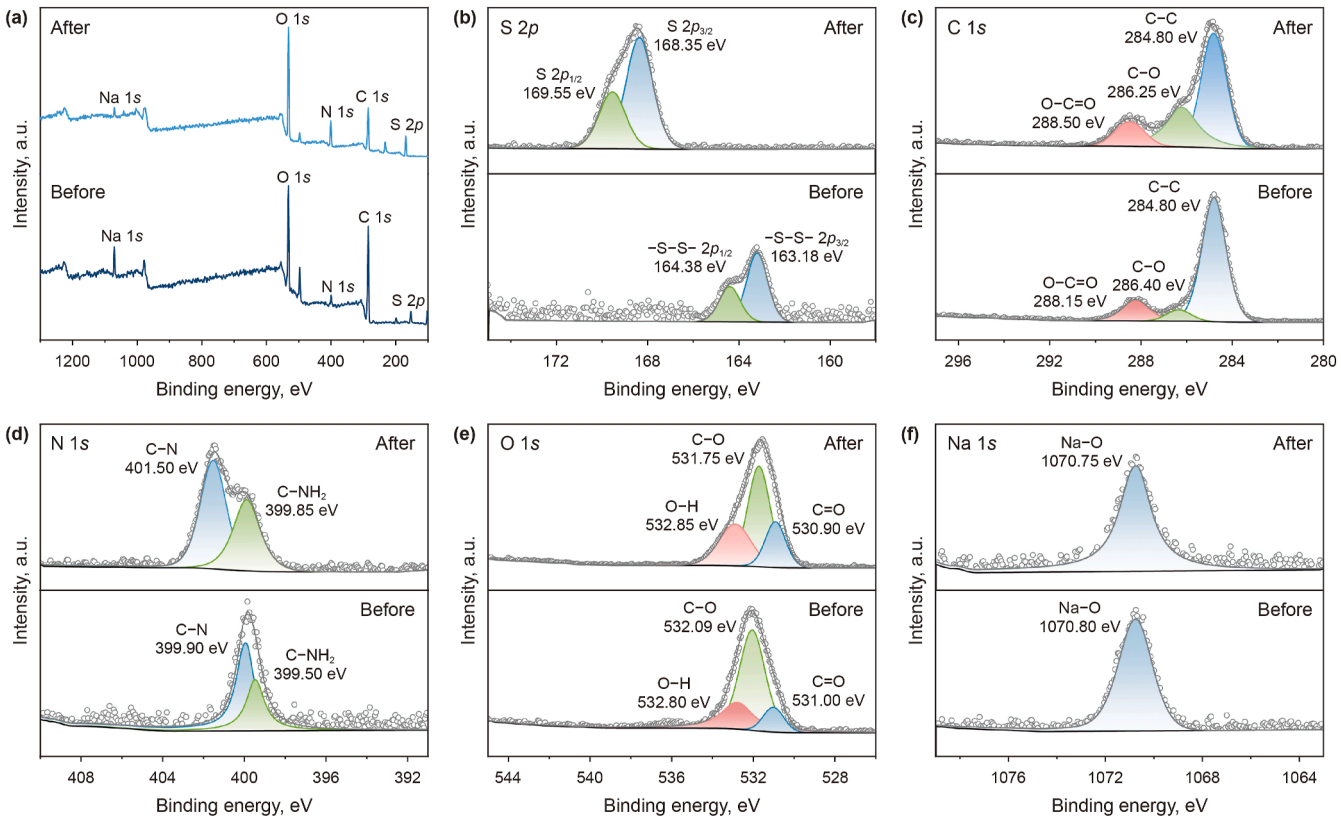


Fig. 8. XPS spectra of DS-PAM before and after degradation: (**a**) full survey spectra; (**b**) S 2*p*; (**c**) C 1*s*; (**d**) N 1*s*; (**e**) O 1*s*; (**f**) Na 1*s*.

3.6. Evaluation of core damage

To evaluate the reservoir damage potential of degraded DS-PAM as a fracturing fluid, this study tested the scaling performance, conductivity, and core damage potential of degraded DS-PAM, and compared them with those of the traditional polymer HPAM (Fig. 9). With the increase in salinity, the scaling rate of HPAM increases significantly. At a salinity of 80,000 mg/L, the

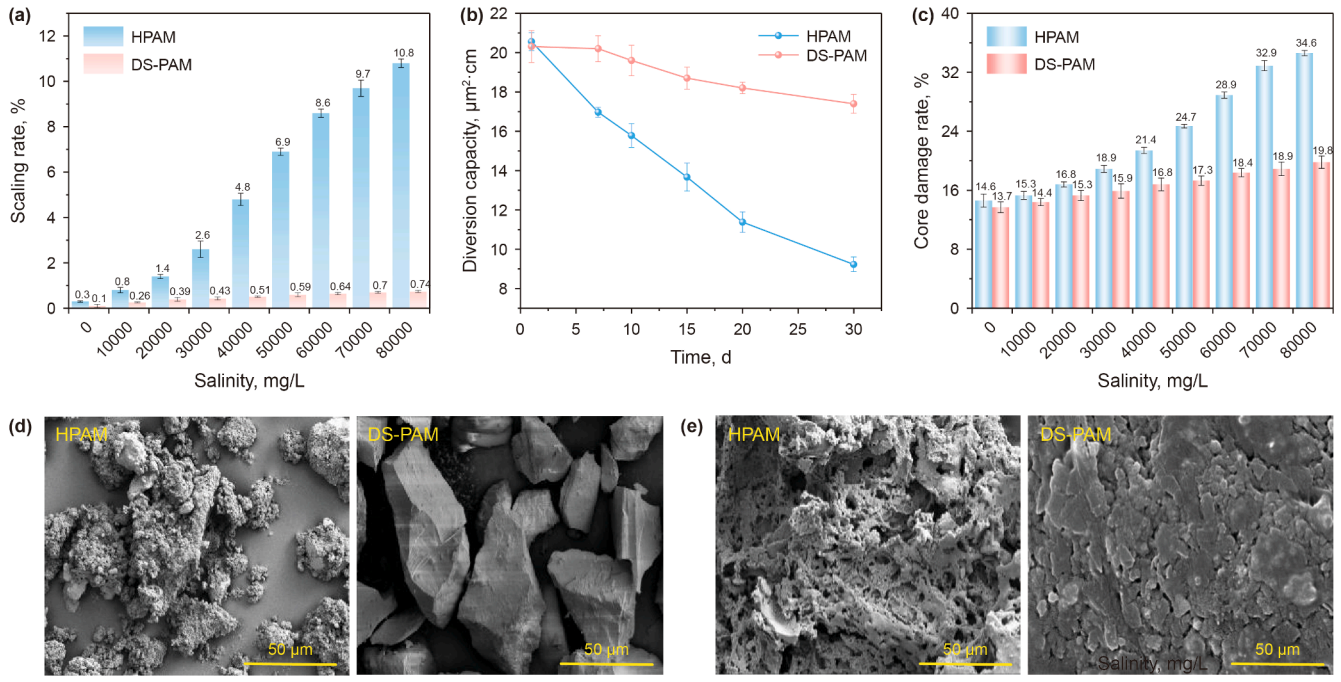


Fig. 9. Comparative performance of HPAM and degraded DS-PAM: (**a**) scaling tendency; (**b**) diversion capacity; (**c**) core damage; (**d**) SEM images of proppants after diversion capacity tests; (**e**) SEM images of core end faces after core damage tests.

scaling rate of HPAM exceeds 10%, while the scaling rate of degraded DS-PAM is minimally affected by salinity and remains consistently below 0.5% (Fig. 9(a)). Thus, degraded DS-PAM fundamentally reduces scaling-induced reservoir damage. The diversion capacity of HPAM decreases from an initial 20.56 to 9.23 $\mu m^2/cm$ (Fig. 9(b)). In contrast, degraded DS-PAM exhibits a slower decreasing trend in diversion capacity with a significantly smaller reduction amplitude compared to HPAM, indicating that degraded DS-PAM possesses superior diversion capacity and stronger stability. The core damage rate of degraded DS-PAM is significantly lower than that of HPAM across all salinity levels. As salinity increases, the core damage rate of degraded DS-PAM rises moderately from 13.7% to 19.8%. This is because metal cations (Ca^{2+}, Mg^{2+}) intensify electrostatic shielding and coiling of DS-PAM molecular chains, reducing their dispersibility, promoting intermolecular hydrophobic association and local aggregation, and forming larger physical aggregates, which in turn diminish effective flow channels and gradually increase core damage. In contrast, the core damage rate of HPAM shows a greater increase, rising significantly from 14.6% to approximately 34.6% (Fig. 9(c)), which demonstrates that degraded DS-PAM causes less damage to the core.

Microscopic analysis was performed on the proppants after diversion capacity and core damage tests. A layer of fluffy, irregular deposits was formed on the surface of the proppants after HPAM testing, whereas no obvious deposits were observed on the surface of the proppants in the DS-PAM group (Fig. 9(d)). A large number of polymer aggregates were detected on the core end face in the HPAM group, whereas the pore structure of the core was still observable in the DS-PAM group (Fig. 9(e)). In summary, degraded DS-PAM exhibits superior performance to HPAM in terms of scaling rate, diversion capacity, and core damage when applied as a fracturing fluid. The main reason is that the degradation of HPAM requires initiation by ammonium persulfate, whose decomposition products contain SO_4^{2-}. These ions combine with divalent cations such as Ca^{2+} and Mg^{2+} in the brine to form deposits, leading to an increase in scaling rate. In contrast, DS-PAM has intrinsic self-degradability, which fundamentally reduces its scaling tendency. Moreover, since the molecular weight of HPAM is significantly higher than that of DS-PAM, it is more prone to causing adsorption damage during diversion capacity and core damage tests. DS-PAM effectively mitigates the reservoir damage caused by traditional polyacrylamide fracturing fluids, and exhibits superior reservoir protection performance. In addition, biological toxicity tests indicate that degraded DS-PAM is non-toxic (Fig. S6(d)). The DS-PAM fracturing fluid combines the low damage advantages of low-polymer fracturing fluids with the low dosage requirement of synthetic polymer fracturing fluids (Table S2), and thus shows great promise for application in oil and gas reservoir fracturing operations.

4. Conclusions

To improve the rheological properties of polyacrylamide-based fracturing fluids and mitigate the flocculation and scaling issues caused by copolymer degradation, a self-degradable polyacrylamide (DS-PAM) with a dual-network structure was successfully synthesized via the innovative incorporation of dynamic covalent bonds. In this system, diallyl dimethyl ammonium chloride (CK-3) forms the first network (physically crosslinked network), while *N*,*N*′-bis(acryloyl)cystamine (BAC) constitutes the second network (chemically crosslinked network). This study systematically investigated the rheological behavior and degradation mechanism of DS-PAM solutions and drew several conclusions.

(1) DS-PAM exhibits exceptional rheological performance. A 0.4 wt% solution exhibits excellent temperature resistance at 120 °C, maintaining a viscosity greater than 30 mPa·s. Furthermore, the prepared fracturing fluid shows outstanding temperature and shear resistance, with a viscosity exceeding 50 mPa·s, and exhibits viscoelastic behavior ($G' > G''$) at 100 °C and a salinity of 40,000 mg/L.

(2) DS-PAM achieves self-degradation without the addition of gel breakers. Kerosene induces dissociation of the hydrophobic association network, whereas high temperature and pH variations trigger cleavage of the covalent network through disulfide bond scission. The degradation process follows the pseudo-first-order kinetic model. The degraded product attains a molecular weight M_v below 200,000 within 48 h.

(3) DS-PAM is a novel low-damage fracturing fluid. Degraded DS-PAM outperforms HPAM in terms of scaling rate (<0.5%) and core damage rate (19.8%), thus causing less reservoir damage. The as-prepared DS-PAM fracturing fluid combines the low-damage advantage of oligomer-based fracturing fluids and the low-addition dosage feature of synthetic polymers, possessing significant theoretical value and promising application prospects.

CRediT authorship contribution statement

Xin Wen: Writing – original draft, Methodology. **Gui-Qiang Fei:** Writing – review & editing, Supervision, Software. **Hua-Qiang Shi:** Supervision, Formal analysis. **Yi-Jie Jiang:** Writing – review & editing. **Guang-Liang Jia:** Data curation. **Jiao-Jiao Zhu:** Writing – original draft, Formal analysis. **Qian-Qian Liu:** Visualization, Software. **Cheng Wang:** Investigation, Formal analysis. **Xiao-Juan Lai:** Writing – review & editing, Formal analysis. **Lei Wang:** Writing – review & editing.

Data availability

Data will be made available on request.

Declaration of competing interest

The authors declare that they have no known competing financial interests or personal relationships that could have appeared to influence the work reported in this paper.

Acknowledgements

This work was financially supported by the Postdoctoral Scientific Research Project of Shaanxi Province (Grant No. 2025BSHSDZZ341), the Service Program for Foreign Experts of Shaanxi Province of China (Grant No. 2023WGZJ-ZD-03), Key R&D Program of Shaanxi Province (Grant No. 2023-YBGY-307), and the National Science and Technology Major Project (Grant No. 2025ZD1404305).

Supplementary data

Supplementary data to this article can be found online at https://doi.org/10.1016/j.petsci.2026.08.017.

References

Almubarak, T., Ng, J.H., Din, H.N.E., Sokhanvarian, K., AlKhaldi, M., 2019. Dual-polymer hydraulic-fracturing fluids: A synergy between polysaccharides and polyacrylamides. SPE J. 24 (6), 2635–2652. https://doi.org/10.2118/191580-PA.

Bai, Y.R., Zhang, Q.T., Sun, J.S., Jiang, G.C., Lv, K.H., 2022. Double network self-healing hydrogel based on hydrophobic association and ionic bond for formation plugging. Pet. Sci. 19 (5), 2150–2164. https://doi.org/10.1016/j.petsci.2022.07.006.

Campos, B.M., Jouenne, J.B., Begrem, S., Chesney, P.J., Mosrati, R., Bréard, J., 2025. Bio-based and biodegradable polymers for composites: Sustainability, challenges, and future perspectives. J. Environ. Chem. Eng. 13 (6), 119306. https://doi.org/10.1016/j.jece.2025.119306.

Duncke, A.C.P., Amaral, C.N.R., Netto, M., Barros, G., Mendes, P.R., Gramatges, A.P., 2026. Coupled effects of sulfonated PAM concentration and degradation on separation kinetics of oil/water emulsions: Interplay of flocculation, viscosity, and homogenization. Fuel 406, 137158. https://doi.org/10.1016/j.fuel.2025.137158.

Fischer, A., Houzelle, M.C., Hubert, P., Axelos, M.A.V., Geoffroy, C.C., Carre, M.C., Viriot, M.L., Dellacherie, E., 1998. Detection of intramolecular associations in hydrophobically modified pectin derivatives using fluorescent probes. Langmuir 14 (16), 4482–4488. https://doi.org/10.1021/la971362w.

Gao, M.W., Zhang, M.S., Du, H.Y., Zhao, M.W., Dai, C.L., You, Q., Liu, S., Jin, Z.H., 2023. A novel triple responsive smart fluid for tight oil fracturing-oil expulsion integration. Pet. Sci. 20 (2), 982–992. https://doi.org/10.1016/j.petsci.2023.01.008.

Ghosh, B., Abdelrahim, M., Ghosh, D., Belhaj, H., 2021. Delayed breaker systems to remove residual polymer damage in hydraulically fractured reservoirs. ACS Omega 6 (47), 31646–31657. https://doi.org/10.1021/acsomega.1c04187.

Grassl, B., Francois, J., Billon, L., 2001. Associating behaviour of polyacrylamide modified with a new hydrophobic zwitterionic monomer. Polym. Int. 50 (10), 1162–1169. https://doi.org/10.1002/pi.751.

Gupta, A.P., Saroop, U.K., Verma, M., 2003. Melt rheological properties of polypropylene/LLDPE copolymer blends. Polym-Plast Technol. 42 (3), 357–372. https://doi.org/10.1081/PPT-120017957.

He, Y., Guo, J., Bai, J., Hua, L., Zhang, Y., Huang, Z., Pan, L., Hong, Z., 2024. An innovative high-strength double-network hydrogel for use as a drilling fluid plugging agent. Gels 10 (4), 224. https://doi.org/10.3390/gels10040224.

Hess, A., Schmidt, B.V., Schlaad, H., 2020. Aminolysis induced functionalization of (RAFT) polymer-dithioester with thiols and disulfides. Polym. Chem. 11 (48), 7677–7684. https://doi.org/10.1039/d0py01365j.

Huang, Q., Liu, S., Cheng, W., Wang, G., 2020. Fracture permeability damage and recovery behaviors with fracturing fluid treatment of coal: An experimental study. Fuel 282, 118809. https://doi.org/10.1016/j.fuel.2020.118809.

Ismail, A., Azadbakht, S., 2024. A comprehensive review of numerical simulation methods for hydraulic fracturing. Int. J. Numer. Anal. Model. 48 (5), 1433–1459. https://doi.org/10.1002/nag.3689.

Jiao, G., Zhu, S., Ye, Z., Shu, Z., Wang, X., Wang, D., 2023. The effect of shear on the properties of an associated polymer solution for oil displacement. Polymers 15 (3), 616. https://doi.org/10.3390/polym15030616.

Jing, Z., Xu, A., Liang, Y.Q., Zhang, Z., Yu, C., Hong, P., Li, Y., 2019. Biodegradable poly (acrylic acid-co-acrylamide)/poly (vinyl alcohol) double network hydrogels with tunable mechanics and high self-healing performance. Polymers 11 (6), 952. https:doi.org/10.3390/polym11060952.

Kaewsaiha, P., Matsumoto, K., Matsuoka, H., 2005. Non-surface activity and micellization of ionic amphiphilic diblock copolymers in water. Hydrophobic chain length dependence and salt effect on surface activity and the critical micelle concentration. Langmuir 21 (22), 9938–9945. https://doi.org/10.1021/la051584r.

Li, W., Merlitz, H., Wu, C.X., Cao, X.Z., 2022. Role of breaking physical crosslinks on safeguarding polymer networks. Phys. Rev. Mater. 6 (12), 123605. https://doi.org/10.1103/PhysRevMaterials.6.123605.

Li, X., Pan, C., Chen, H., Zhang, Z., Ning, K., 2025a. Preparation and performance evaluation of temperature-and salt-resistant hydrophobically associated polymer fracturing fluids. ACS Omega 10 (8), 8281–8291. https://doi.org/10.1021/acsomega.4c10023.

Li, X., Ye, Z., Luo, P., 2025b. Performance evaluation of enhanced oil recovery by host-guest interaction of β-cyclodextrin polymer/hydrophobically associative polymer. Molecules 30 (1), 109. https://doi.org/10.3390/molecules30010109.

Liu, A.Q., Liu, L.J., Xu, W.S., Xu, X.L., Chen, J.Z., An, L.J., 2021. Stress-structure relationship of the reversible associating polymer network under start-up shear flow. Chin. J. Polym. Sci. 39, 387–396. https://doi.org/10.1007/s10118-020-2487-6.

Liu, T., Chen, X., Tang, X., 2025. Reservoir compatibility and enhanced oil recovery of polymer and polymer/surfactant system: Effects of molecular weight and hydrophobic association. Polymers 17 (10), 1390. https://doi.org/10.3390/polym17101390.

Liu, Z.R., Tan, L.L., Gao, J., Qin, Z.Y., Huo, X.X., Liang, Z.M., 2024. Hydrophobically modified polyacrylamide incorporating both hydrophilic and hydrophobic units: Enhanced printability and stability in aqueous ink. Molecules 29 (21), 5105. https://doi.org/10.3390/molecules29215105.

Maruya, L.K., Shetty, C., Jazani, A.M., Arezi, N., Oh, J.K., 2020. Dual reduction/acid-responsive disassembly and thermoresponsive tunability of degradable double hydrophilic block copolymer. ACS Omega 5 (7), 3734–3742. https://doi.org/10.1021/acsomega.9b04430.

Moad, G., Rizzardo, E., Thang, S.H., 2005. Living radical polymerization by the RAFT process. Aust. J. Chem. 58 (6), 379–410. https://doi.org/10.1071/CH05072.

Narimani, A., Kordnejad, F., Hemmati, M., Duong, A., 2022. Synthesis, characterization, and rheological behavior of HPG graft poly (AM-co-AMPS)/GO nanocomposite hydrogel system for enhanced oil recovery. Dispersion Sci. Technol. 185, 26–38. https://doi.org/10.1080/01932691.2022.2125876.

Pitt, C.G., Gu, Z., 1987. Modification of the rates of chain cleavage of poly(ϵ-caprolactone) and related polyesters in the solid state. J. Controlled Release 4 (4), 283–292. https://doi.org/10.1016/0168-3659(87)90020-4.

Pitt, C.G., Chasalow, F.I., Hibionada, Y.M., Klimas, D.M., Schindler, A., 1981. Aliphatic polyesters. I. The degradation of poly(ϵ-caprolactone) in vivo. J. Appl. Polym. Sci. 26 (11), 3779–3787. https://doi.org/10.1002/app.1981.070261124.

Rosenbloom, S.I., Sifri, R.J., Fors, B.P., 2021. Achieving molecular weight distribution shape control and broad dispersities using RAFT polymerizations. Polym. Chem. 12 (34), 4910–4915. https://doi.org/10.1039/d1py00399b.

Santos, J.F., Santos, A.S., Oliveira, P.F.D., Santos, I.C.V.M., Mansur, C.R.E., 2024. Statistical and rheological evaluation of the effect of salts in partially hydrolyzed polyacrylamide solutions. J. Appl. Polym. Sci. 141 (17), e55278. https://doi.org/10.1002/app.55278.

Shao, Y., Mao, J., Yang, B., Zhao, J., Yang, X., 2020. High performance hydrophobic associated polymer for fracturing fluids with low-dosage. Pet. Chem. 60, 219–225. https://doi.org/10.1134/s0965544120020115.

Sun, M., Xu, Z., Munyaneza, N.E., Zhang, Y., Posada, C., Liu, G., 2023. Solvent-induced competing processes in polycarbonate degradation: Depolymerization, chain scission, and branching/crosslinking. Polym. Chem. 14 (16), 1915–1922. https://doi.org/10.1039/d2py01572b.

Takahashi, A., Ohishi, T., Goseki, R., Otsuka, H., 2016. Degradable epoxy resins prepared from diepoxide monomer with dynamic covalent disulfide linkage. Polymer 82, 319–326. https://doi.org/10.1016/j.polymer.2015.11.057.

Telin, A., Lenchenkova, L., Yakubov, R., Poteshkina, K., Krisanova, P., Filatov, A., Stefantsev, A., 2023. Application of hydrogels and hydrocarbon-based gels in oil production processes and well drilling. Gels 9 (8), 609. https://doi.org/10.3390/gels9080609.

Wang, W., Zhou, Z., Sathe, D., Tang, X., Moran, S., Jin, D.J., Haeffner, D.F., Wang, P.J., Niu, P.J., 2022. Degradable vinyl random copolymers via photocontrolled radical ring-opening cascade copolymerization. Angew. Chem. Int. Ed. 61 (8), e202113302. https://doi.org/10.1002/anie.202113302.

Wang, W., Rondon, B., Wang, Z., Wang, J., Niu, J., 2023. Macrocyclic allylic sulfone as a universal comonomer in organocatalyzed photocontrolled radical copolymerization with vinyl monomers. Macromolecules 56 (5), 2052–2061. https://doi.org/10.1021/acs.macromol.2c02025.

Yang, K., Wang, F.Y., Zhao, J.Y., 2023. Experimental study of surfactant-enhanced spontaneous imbibition in fractured tight sandstone reservoirs: The effect of fracture distribution. Pet. Sci. 20 (1), 370–381. https://doi.org/10.1016/j.petsci.2022.09.033.

Ye, L., Lv, Q., Sun, X., Liang, Y., Fang, P., Yuan, X., Li, M., Zhang, X., Shang, X., Liang, H., 2020. Fully physically cross-linked double network hydrogels with strong mechanical properties, good recovery and self-healing properties. Soft Matter 16 (7), 1840–1849. https:doi.org/10.1039/c9sm02071c.

Zhang, N., Pan, X., Xi, A., Chen, W., Huang, T., Zeng, Y., 2024a. Robust, malleable, degradable, self-healable, weldable and recyclable polyimine thermosets from natural peach gum and chitosan. Polym. Chem. 15 (32), 3287–3299. https://doi.org/10.1039/d4py00473f.

Zhang, Q., Li, J., 2022. Force-extension curve of a polymer chain entangled with a static ring-shaped obstacle. Polymers 14 (22), 4613. https://doi.org/10.3390/polym14214613.

Zhang, X., Guo, J., Fei, D., Wang, L., Peng, Z., Li, J., Dong, J., 2024b. Polymer surfactants as viscosity reducers for ultra-heavy oil: Synthesis and viscosity reduction mechanism. Fuel 357, 129871. https://doi.org/10.1016/j.fuel.2023.129871.

Zhang, Y., Xu, T., Peng, F., Cao, R., Liu, Z., Sun, H., Cui, K., Li, L., 2025. Investigating hydrogen bonding in poly(vinyl butyral) copolymers near glass-transition temperature under uniaxial stress: A coarse-grained molecular dynamics study. Soft Matter 21 (29), 5980–5989. https://doi.org/10.1039/d5sm00431d.

Zhao, B., Zhao, M., Li, L., Sun, S., Yu, H., Cheng, Y., Yang, Y., Fan, Y., Sun, Y., 2022. Preparation and properties of double-crosslinked hydroxyapatite composite hydrogels. Int. J. Mol. Sci. 23 (17), 9962. https://doi.org/10.3390/ijms23179962.

Zhong, C., Huang, R., Zhang, X., Dai, H., 2007. Synthesis, characterization, and solution properties of an acrylamide-based terpolymer with butyl styrene. J. Appl. Polym. Sci. 103 (6), 4027–4038. https://doi.org/10.1002/app.25546.

Zhou, H., Song, G.Q., Guo, J.F., Zhang, Y.X., Dieing, R., Ma, L., Haeussling, L., 2010. Hydrophobically modified polyelectrolytes: V. Interaction of fluorocarbon modified poly(acrylic acid) with various added surfactants. Chin. J. Chem. 19 (8), 745–750. https://doi.org/10.1002/cjoc.20010190807.